




# Design of a novel detector based on photonic crystal nanostructure for ultra-high performance detection of cells with diabetes

Malek G. Daher<sup>1</sup> · Zbigniew Jaroszewicz<sup>2,3</sup> · Samer H. Zyoud<sup>4,5,6</sup> · Abinash Panda<sup>7</sup> · SK Hasane Ahammad<sup>8</sup> · Mohammed Abd-Elnaby<sup>9</sup> · Mahmoud M. A. Eid<sup>10</sup> · Ahmed Nabih Zaki Rashed<sup>11</sup> 

Received: 27 April 2022 / Accepted: 10 August 2022 / Published online: 13 September 2022

© The Author(s), under exclusive licence to Springer Science+Business Media, LLC, part of Springer Nature 2022

## Abstract

Diabetes is becoming a global problem since it is the leading cause of mortality for many people all over the world. As a result, a diabetes sensor that is accurate, quick, and sensitive is required. On the basis of a binary photonic crystal, a new bio-photonic detector has been built for sensing diabetes-affected cells. It has two layers of Ge and TiN, with a defect cavity chosen as a sample and placed in the middle. The suggested biosensor's detecting mechanism is based on altering the refractive index of the sensing sample, which causes a shift in the location of the resonant peak inside the photonic band gap of transmittance spectra. The suggested structure's transmittance qualities are examined using the transfer matrix approach. The impact of incidence angle (TE and TM polarization) and defect cavity thickness on the performance of our proposed biosensor has been investigated. The suggested biosensor has a sensitivity of 2676.66 nm/RIU at optimal conditions, which is exceptionally high when compared to several previous studies. In addition, the suggested biosensor with a very low detection limit has an ultra-high-quality factor and figure of merit. Furthermore, the suggested detector is simple to fabricate and has a low-cost structure, making it appealing for use in a variety of bio-sensing applications.

**Keywords** Photonic crystal · Effected cells of diabetes · Biosensor · Transmittance spectra · Defect cavity

## 1 Introduction

Diabetes is an illness that can be fatal. Over 415 million individuals are impacted globally. It is anticipated that by 2040, this number would reach 642 million (Bommer et al. 2017). Diabetes is the primary killer of people between the ages of 20 and 59. When the body's blood sugar levels cannot be managed, diabetes develops. There are two types of diabetes: type 1 and type 2. When a person has type 1 diabetes, their body is unable to

---

✉ Ahmed Nabih Zaki Rashed  
ahmed\_733@yahoo.com

Extended author information available on the last page of the article

generate the hormone insulin, which is necessary to control blood sugar levels. For the body to convert glucose molecules into energy, insulin is necessary (Haxha and Jhoja 2016). Type 2 diabetes develops when the body either generates insufficient insulin or insulin that the body rejects (Almawgani et al. 2022a). Adults over the age of 40 are the most affected. Globally, class-2 diabetes is growing at a higher rate than class-1 diabetes (Bommer et al. 2017; Haxha and Jhoja 2016; Almawgani et al. 2022a). The body is affected by diabetes in many different ways. It contributes to a number of major issues, such as heart disease and visual issues, renal troubles, brain malfunctions, and early death. It's also become one of the most prevalent causes of injury-related limb amputations. Diabetes-related kidney and heart disease are on the rise, killing thousands of people each year (Almawgani et al. 2022a). It is critical to create a sensitive and real-time diabetes detector based on the aforementioned details.

Due to their unique properties, photonic crystals (PCs) have recently shown an intriguing response to the regulation of electromagnetic wave propagation. PCs can constrain or permit the transmission of incident light by providing pass or stop bands of frequencies (Taya et al. 2022; Elsayed et al. 2021; Zhang and Li-Ping 2014; Threm et al. 2012). Photonic band gaps (PBGs) are the names for these bands. As a consequence of the PBG (Xie et al. 2017; Fu et al. 2019; Sánchez and Orozco 2016; Qin et al. 2012; Harding et al. 2009), A variety of optical devices, including reflectors, detectors, and switches, have been made using PCs. Thus, PCs may have a considerable influence on the development of biosensor performance. In a recent study (Zyoud and Ahmed 2022; Panda et al. 2018), the authors constructed a 1D photonic structure and thoroughly investigated the impact of different types of losses that happen during light signal transmission through the apparatus. Photonic structures have been used to detect protein, DNA, sodium chloride, and urea. Amiri et al. (2019), Tang and Wang (2008), notably as glucose sensors (Frischeisen et al. 2008), urea level sensors (Chow et al. 2004), and blood biosensors (Almawgani et al. 2022b; Ramanujam et al. 2019). These optical biosensors are very good at what they do and respond quickly to even small changes in what they are looking for Aly et al. (2018), Avsar (2015).

A binary photonic crystal (BPhC) made up of two periodic layers of Ge and TiN is presented in this work as a real-time biosensor for detecting diabetes-affected cells. The suggested structure's transmittance qualities are examined using the transfer matrix approach. The effects of incidence angle (TE and TM polarizations) and defect cavity thickness on the suggested biosensor's performance have been investigated. The best possible scenario for the BPhC sensor is calculated and compared to the most up-to-date biosensor-related detectors.

## 2 Design and Theoretical Simulation

A binary photonic crystal (BPhC) is made up of the structures  $(\text{Ge}/\text{TiN})^N$  (sensing layer) and  $(\text{Ge}/\text{TiN})^N$  as shown in Fig. 1. This structure is recommended for detecting diabetes-affected cells. The BPhC is surrounded on all sides by air. The thicknesses of the Ge and TiN layers are measured using Bragg's quarter wavelength, and  $N = 4$  is chosen as the number of cells (periods).

Here, the transmittance spectrum was investigated using the transfer matrix technique. The typical transfer matrices are described in the following way:

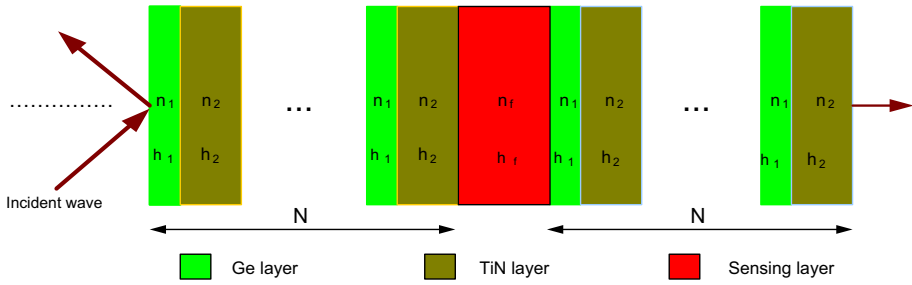


**Fig. 1** A schematic representation of a faulty binary photonic crystal with a defect cavity made up of a sensing layer

$$Q_j = \begin{bmatrix} \cos(\aleph_j) & -\frac{i \sin(\aleph_j)}{G_j} \\ -iG_j \sin(\aleph_j) & \cos(\aleph_j) \end{bmatrix} \tag{1}$$

$\aleph_j$  is defined as the propagating light wave phase variation through the  $j$ th layer.

$$\aleph_j = \frac{2\pi}{\lambda} n_j h_j \cos \theta_j \tag{2}$$

where  $n_j$  is the layer’s index of refraction and  $h_j$  is its thickness,  $\theta_j$  is the layer’s incidence angle, which is represented as:

$$\cos \theta_j = \sqrt{1 - \left(\frac{n_0 \sin(\theta_0)}{n_j}\right)^2} \tag{3}$$

For transverse electrical (TE) waves,  $G_j = n_j \cos(\theta_j)$ , but for alternating magnetic (TM) waves,  $G_j = \cos(\theta_j)/n_j$ , where  $n_0$  is the refractive index of the surrounding medium. For one cell with A and B layers, the transfer matrix  $Q_0$  may be written as  $Q_0 = Q_A Q_B$ . A defective binary photonic crystal’s entire transfer matrix  $Z$  may be written as:

$$Z = (Q_0)^N Q_D (Q_0)^N = \begin{bmatrix} Z_{11} & Z_{12} \\ Z_{21} & Z_{22} \end{bmatrix} \tag{4}$$

where  $Q_D$  is the defect cavity’s transfer matrix and  $Z_{ij}$  is the entire transfer matrix  $Z$ ’s elements. The coefficient of transmission ( $t$ ) and the transmittance ( $T$ ) are calculated as follows:

$$t = \frac{2G_{in}}{(Z_{11} + Z_{12}G_s)G_{in} + (Z_{21} + Z_{22}G_s)} \tag{5}$$

$$T = \frac{G_s}{G_{in}} |t|^2 \tag{6}$$

The reflection coefficient ( $r$ ) and the reflectance ( $R$ ) can be expressed as:

$$r = \frac{(Z_{11} + Z_{12}G_s)G_{in} - (Z_{21} + Z_{22}G_s)}{(Z_{11} + Z_{12}G_s)G_{in} + (Z_{21} + Z_{22}G_s)} \quad (7)$$

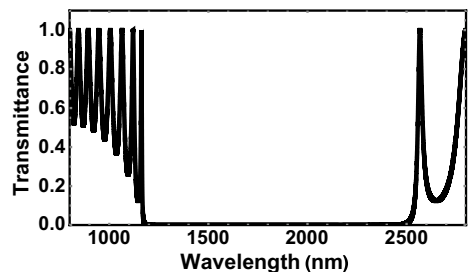
$$R = |r|^2 \quad (8)$$

$G_s = n_s \cos(\theta_s)$  and  $G_{in} = \cos(\theta_0)$  for transverse electrical (TE) wave.

### 3 Numerical analyses and discussion

The transmittance properties of a 1D-binary photonic crystal (BPhC) are explored utilizing the transfer matrix method (TMA) and mathematica simulation. The recommended BPhC configuration is  $\text{air}/(\text{Ge}/\text{TiN})^4$  (sensing layer)  $(\text{Ge}/\text{TiN})^4/\text{air}$ . Several dielectrics and semi-conducting materials are employed to structure photonic crystals. Here we choose the germanium and titanium nitride because of the large difference in refractive indices between the Ge and TiN layers. As a result, a photonic band gap with a large width will be created. Also, it is expected the efficiency of those crystals will improve as optical sensors. The sensing layer is either a normal cell or a diabetic cell infected with 1.350 and 1.410 refractive indices, respectively (Sani et al. 2021). It is worth mentioning that the substrate will take part in the optical path and contribute to the overall transmittance. However, the substrate material does not have an appreciable effect on the resulting spectrum. Thus, it will almost no effect on the achievement of the photo-detector. So the crystal is surrounded on all sides by air. In order to develop an efficient sensor with excellent efficiency, the influence of incidence angle (TE and TM modes) and sensing layer thickness are investigated. In numerical calculations, the indices of refraction for Ge and TiN layers are  $n_1 = 4.23$  and  $n_2 = 1.2887$ , respectively. These layers' thicknesses ( $h_1 = 106.38$  nm,  $h_2 = 349.18$  nm) are chosen as quarter wavelengths, with  $\lambda_0 = 1800$  nm as the center wavelength. Photonic crystals can operate in both the visible light and infrared region of incident electromagnetic waves. Here the infrared source (IR- source) is suitable for acquisition of the used wavelengths. For example, As an infrared source, a tuneable carbon dioxide laser is employed to detect specific air pollutants and identify absorbing kinds in aqueous solutions. On other hand, an infrared spectrophotometer is a device that emits infrared light into a substance. It then generates a spectrum with a graph that contrasts the amount of light transmitted (on the vertical axis) with the wavelength (on the horizontal axis). Figure 2 shows the transmittance spectrum through the proposed BPhC without any sensing layer. There is a photonic band gap created. The right and left borders of the photonic band gap are at wavelengths of 2542.57 nm and 1176.24 nm, respectively, while the breadth of the photonic band gap

**Fig. 2** The transmission spectrum of a suggested BPhC with no defect cavity at ( $h_1 = 106.38$  nm,  $h_2 = 349.18$  nm,  $n_1 = 4.23$ ,  $n_2 = 1.2887$ ,  $\theta_0 = 0.0^\circ$ , and  $N = 4$ )



can reach 1366.33 nm. When a normal cell and a diabetes-affected cell are regarded as defect layers with a thickness of  $h_d = 500$  nm, the transmittance spectra through the suggested structure are shown in Fig. 3. The left and right borders of the photonic band gap have been discovered to be at wavelengths of 1202.64 nm and 2727.39 nm, respectively. As a result, the breadth of the photonic band gap widens to 1524.57 nm. Multiple Bragg scattering occurs between incident, reflected, and scattered electromagnetic waves, resulting in these photonic band gaps. When the normal cells of diabetes (NCD) are treated as a defect cavity, a resonant peak may be noticed at a wavelength of 1976.62 nm. When the affected cells of diabetes (ECD) are chosen as a defect layer, the resonant peak shifts to a greater wavelength, as illustrated in Fig. 3. The resonant peak has moved to a wavelength of 2019.22 nm. The situation of a standing wave (Taya et al. 2021) can explain this red shift.

$$OPD = n_{eff}Q = b\lambda \quad (9)$$

The difference of optical path, effective index, difference of geometric path, and an integer number are represented by  $OPD$ ,  $n_{eff}$ ,  $Q$ , and  $b$ , respectively. At normal incidence, the suggested detector is found to have a sensitivity of roughly 710 nm/RIU. The impact of incidence angle and defect cavity thickness will be explored and optimized in the following phases.

### 3.1 Influence of the incident angle

The transmittance spectra for both (TE and TM modes) have been investigated at  $h_d = 500$  nm at various incidence angles. In the first, it is evident that when the angle of incidence increases, the location of the resonant peak for both TE and TM modes has been shifted to the left. According to the Bragg-Snell law (Daher et al. 2022a), this blue shift can be explained.

$$a\lambda = 2G(n_{eff}^2 - \sin^2 \theta_0)^{0.5} \quad (10)$$

where  $a$ ,  $\lambda$ ,  $G$ ,  $n_{eff}$ ,  $\theta_0$  are the order of diffraction ( $a = 1, 2, 3, \dots$ ), the wavelength, the inter-planar spacing, the effective refractive index and the incident angle, respectively. As a result, the angle of incident light has a significant influence on the efficiency parameters of bio-photonic detector. Now, the various parameters have been examined, including sensitivity (S), figure of merit (FOM), quality factor (QF) and detection limit (DL), to see how well the suggested structure performed as a biosensor. The sensitivity (S) can be evaluated

**Fig. 3** The Transmittance spectra of a suggested BPhC with defect layer (NCD and ECD) at ( $h_1 = 106.38$  nm,  $h_2 = 349.18$  nm,  $h_d = 500$  nm,  $n_1 = 4.23$ ,  $n_2 = 1.2887$ ,  $\theta_0 = 0^\circ$ , and  $N = 4$ )

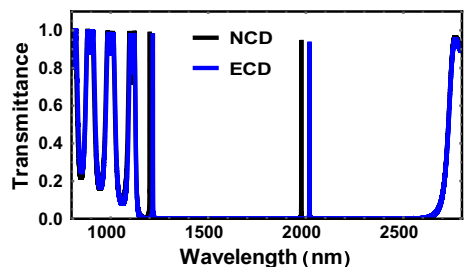


**Table 1** The incidence angle affects the position of the resonant peak and the sensitivity of the proposed structure (TE mode)

Incident angle (degree)	Position of defect peak of NCD (nm)	Position of defect peak of ECD (nm)	Shift of wave-length (nm)	Sensitivity (nm/RIU)
0.0	1976.62	2019.22	42.6	710
10	1964.49	2007.82	43.33	722.16
20	1928.55	1974.06	45.51	758.5
30	1870.33	1919.54	49.21	820.16
40	1792.96	1847.48	54.52	908.66
50	1702.07	1763.33	61.26	1021
60	1606.83	1675.84	69.01	1150.16
70	1520.55	1597.20	76.65	1277.5
80	1459.13	1541.69	82.56	1376

**Table 2** Variation of resonant peak position and sensitivity of the proposed structure with the incidence angle (TM mode)

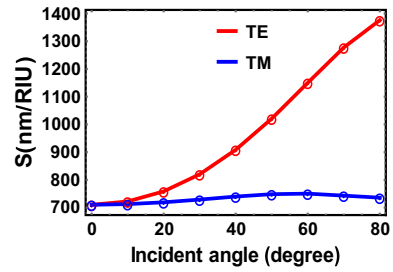
Incident angle (degree)	Position of defect peak of NCD (nm)	Position of defect peak of ECD (nm)	Shift of wavelength (nm)	Sensitivity (nm/RIU)
0.0	1976.62	2019.22	42.6	710
10	1961.37	2004.12	42.75	712.5
20	1916.81	1959.95	43.14	719
30	1846.59	1890.32	43.73	728.83
40	1756.85	1801.24	44.39	739.83
50	1656.46	1701.36	44.9	748.33
60	1556.87	1601.89	45.02	750.33
70	1471.41	1516	44.59	743.16
80	1413.36	1457.5	44.14	735.66

by Eq. (11) (Daher et al. 2022b). It says that the fraction of the shift in position of resonant wavelength ( $\Delta\lambda$ ) and the refractive index changes ( $\Delta n$ ) can be used to figure this out.

$$S = \frac{\Delta\lambda}{\Delta n} \quad (11)$$

In our calculations,  $\Delta\lambda = \lambda_{ECD} - \lambda_{NCD}$  and  $\Delta n = n_{ECD} - n_{NCD}$ . When the incidence angle varies from  $0.0^\circ$  to  $80^\circ$  for TE polarization, the sensitivity rises from 710 nm/RIU to 1376 nm/RIU, as shown in Table 1. The defect peak is not visible when the angle of incidence exceeds  $\theta_0 = 80^\circ$ . As a result,  $\theta_0 = 80^\circ$  was chosen as the best incidence angle. When the incidence angle ranges from  $0.0^\circ$  to  $60^\circ$ , the sensitivity of TM polarization rises from 710 nm/RIU to 750.33 nm/RIU before dropping as indicated in Table 2. Figure 4 depicts the evolution of sensitivity for TE polarization, which is higher than TM polarization, as the incidence angle increases, which is an important goal in the design of optical sensing systems. The ratio between the location of the defect peak ( $\lambda_{peak}$ ) and the full width half maximum (FWHM) for this crest can be used to calculate the quality factor (QF) by using Eq. (12) (Daher et al. 2022b):

**Fig. 4** The Sensitivity (S) vs the incidence angle of a suggested BPhC for both TE and TM modes at ( $h_1 = 106.38$  nm,  $h_2 = 349.18$  nm,  $h_d = 500$  nm,  $n_1 = 4.23$ ,  $n_2 = 1.2887$ , and  $N = 4$ )



$$QF = \frac{\lambda_{peak}}{FWHM} \tag{12}$$

The potential to sense any alteration in index is represented by (FOM), which is determined as a ratio between the sensitivity (S) and (FWHM) of the defect peak using the following expression (Daher et al. 2022b):

$$FOM = S / FWHM \tag{13}$$

Table 3 (TE polarization) and Table 4 (TM polarization) show the numerical findings of quality factor and figure of merit at various angles ranging from 0.0° to 80° in 10° steps. As demonstrated in Figs. 5 and 6, when the angle of incidence varies from 0.0° to 80° for TE polarization, both *QF* and *FOM* increase, whereas they decrease for TM polarization. This indicates that TE polarization’s defect peaks are sharper than TM polarization’s, which is one of the key requirements for any successful optical detector. The fourth parameter is the DL, which is described as the smallest refractive index change that can be properly detected. Equation (14) was used to determine this factor (*DL*) (Daher et al. 2022b).

$$DL = \left(\frac{2\Delta n}{3}\right) \left(\frac{FWHM}{\Delta\lambda}\right)^{\frac{5}{4}} \tag{14}$$

**Table 3** Variation of *FWHM*, *QF*, *FOM* and *DL* of the proposed structure with the incidence angle (TE mode)

Incident angle (degree)	<i>FWHM</i> (nm)	<i>QF</i>	<i>FOM</i> (RIU <sup>-1</sup> )	<i>DL</i> (RIU)
0.0	0.47	4296.21	1510.63	1.43 × 10 <sup>-4</sup>
10	0.43	4669.34	1679.45	1.25 × 10 <sup>-4</sup>
20	0.39	5061.69	1944.87	1.04 × 10 <sup>-4</sup>
30	0.30	6398.46	2733.88	6.81 × 10 <sup>-5</sup>
40	0.20	9237.4	4543.33	3.61 × 10 <sup>-5</sup>
50	0.14	12,595.21	7292.85	1.99 × 10 <sup>-5</sup>
60	0.11	15,234.90	10,456.06	1.27 × 10 <sup>-5</sup>
70	0.10	15,972	12,775	9.91 × 10 <sup>-6</sup>
80	0.04	38,542.25	34,400	2.87 × 10 <sup>-6</sup>

**Table 4** Variation of *FWHM*, *QF*, *FOM* and *DL* of the proposed structure with the incidence angle (TM mode)

Incident angle (degree)	<i>FWHM</i> (nm)	<i>QF</i>	<i>FOM</i> ( <i>RIU</i> <sup>-1</sup> )	<i>DL</i> ( <i>RIU</i> )
0.0	0.47	4296.21	1510.63	$1.43 \times 10^{-4}$
10	0.49	4090.04	1454.08	$1.50 \times 10^{-4}$
20	0.5	3919.9	1438	$1.52 \times 10^{-4}$
30	0.58	3259.17	1256.60	$1.80 \times 10^{-4}$
40	0.71	2536.95	1042.01	$2.27 \times 10^{-4}$
50	1.05	1620.34	712.69	$3.65 \times 10^{-4}$
60	1.58	1013.85	474.89	$6.07 \times 10^{-4}$
70	2.71	559.40	274.23	$12.07 \times 10^{-4}$
80	5.05	288.61	145.67	$26.61 \times 10^{-4}$

**Fig. 5** The Quality Factor (*QF*) vs the incidence angle of a suggested BPhC for both TE and TM modes at ( $h_1 = 106.38$  nm,  $h_2 = 349.18$  nm,  $h_d = 500$  nm,  $n_1 = 4.23$ ,  $n_2 = 1.2887$ , and  $N = 4$ )

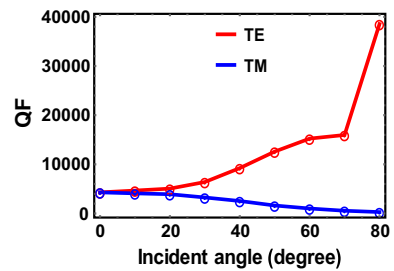
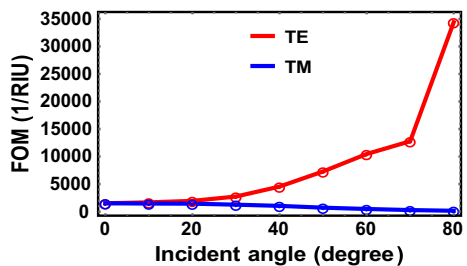


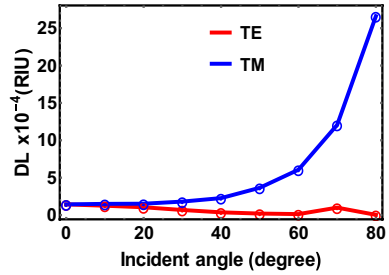
**Fig. 6** Figure of merit (*FOM*) vs the incidence angle of a proposed binary photonic crystal for both TE and TM modes at ( $h_1 = 106.38$  nm,  $h_2 = 349.18$  nm,  $h_d = 500$  nm,  $n_1 = 4.23$ ,  $n_2 = 1.2887$ , and  $N = 4$ )



When the angle of incidence changes from  $0.0^\circ$  to  $80^\circ$ , the *DL* for TE polarization declines while it climbs for TM polarization, as illustrated in Fig. 7. The value of *DL* is extremely low, implying that the suggested biosensor can detect even small changes in the refractive index of the sensing layer. From the above data, we can conclude that performance of the suggested biosensor depending upon the incident angle. The detector performance is equal for both TE and TM polarizations at the normal incidence. Utilizing higher incidence angles leads to a significant improvement in the performance of the optical detector in the case of TE polarization, while the performance is reduced in the



**Fig. 7** Detection Limit (DL) versus the incidence angle of a proposed BPhC for both TE and TM modes at ( $h_1 = 106.38$  nm,  $h_2 = 349.18$  nm,  $h_d = 500$  nm,  $n_1 = 4.23$ ,  $n_2 = 1.2887$ , and  $N = 4$ )



case of TM polarization. As a result, it is clear that TE polarization is preferable to TM polarization for the suggested bio-photonic detector design. Thus, the next investigation will use TE polarization.

### 3.2 Influence of the defect cavity thickness

The transmittance spectra of the defect cavity at various thicknesses are also examined. From Eq. (9), any variation in the refractive index of defect cavity leads to a variation in the defect mode location. On other hand, as the thickness of defect cavity rises, the wave will have a longer geometric path through the cavity and a greater interaction occurs between the incident wave and the analyte. Therefore, the thickness of the defect cavity into a photonic crystal has a meaningful effect on the performance of bio-photonic detector (Aly and Zaky 2019). The sensitivity improved from 1376 to 2688.33 nm/RIU when the angle of incidence was set at  $\theta_0 = 80^\circ$  (the optimal value) and the thickness of the defect cavity was adjusted from 500 to 7000 nm, as shown in Table 5. These findings are in line with a number of recently published articles. Figure 8 displays the sensitivity versus defect cavity thickness. As shown in Table 6, the QF and FOM fluctuate with increasing the thickness of the fault cavity. As demonstrated in Figs. 9 and 10, the greatest QF of 104,337.5 and FOM of 133,833.3 RIU<sup>-1</sup> are found at defect cavity thicknesses of 5000 nm, respectively.

**Table 5** Variation of the suggested structure’s resonant peak position and sensitivity with defect cavity thickness

Defect cavity thickness (nm)	Defect peak position of NCD (nm)	Defect peak position of ECD (nm)	Shift of wave-length (nm)	Sensitivity (nm/RIU)
500	1459.13	1541.69	82.56	1376
1000	2140.94	2250.73	109.79	1829.83
2000	2024.36	2165.86	141.5	2358.33
3000	1972.81	2125.09	152.28	2538
4000	1944.27	2101.74	157.47	2624.5
5000	1926.23	2086.69	160.6	2676.66
6000	2260.68	2421.5	160.82	2680.33
7000	2269	2430.3	161.3	2688.33

**Fig. 8** Sensitivity ( $S$ ) vs the defect cavity thickness ( $h_d$ ) of a proposed BPhC for TE mode at ( $h_1 = 106.38$  nm,  $h_2 = 349.18$  nm,  $n_1 = 4.23$ ,  $n_2 = 1.2887$ ,  $\theta_0 = 80^\circ$ , nm and  $N = 4$ )

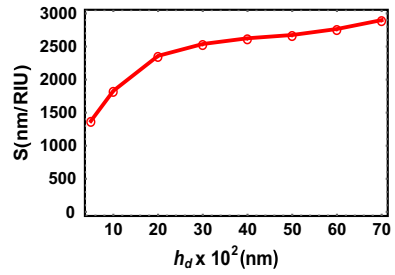


**Table 6** Variation of  $FWHM$ ,  $QF$ ,  $FOM$  and  $DL$  of the proposed structure with the defect layer cavity thickness

Defect layer thickness (nm)	$FWHM$ (nm)	$QF$	$FOM$ ( $RIU^{-1}$ )	$DL$ ( $RIU$ )
500	0.04	38,542.25	34,400	$2.87 \times 10^{-6}$
1000	0.4	5626.825	4574.58	$3.58 \times 10^{-5}$
2000	0.13	16,660.46	18,141.02	$6.39 \times 10^{-6}$
3000	0.06	35,418.16	42,300	$2.22 \times 10^{-6}$
4000	0.05	42,034.8	52,490	$1.69 \times 10^{-6}$
5000	0.02	104,337.5	133,833.3	$5.26 \times 10^{-7}$
6000	0.37	6544.32	7230.18	$1.93 \times 10^{-5}$
7000	0.39	6054.33	6977.35	$1.95 \times 10^{-5}$

**Fig. 9** Quality Factor ( $QF$ ) vs the defect cavity thickness ( $h_d$ ) of a proposed BPhC for TE mode at ( $h_1 = 106.38$  nm,  $h_2 = 349.18$  nm,  $n_1 = 4.23$ ,  $n_2 = 1.2887$ ,  $\theta_0 = 80^\circ$ , nm and  $N = 4$ )

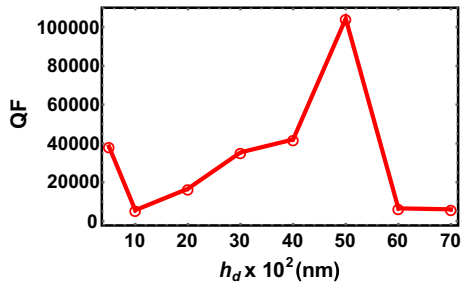


**Fig. 10** Figure of merit ( $FOM$ ) vs the defect cavity thickness ( $h_d$ ) of a proposed binary photonic crystal for TE mode at ( $h_1 = 106.38$  nm,  $h_2 = 349.18$  nm,  $n_1 = 4.23$ ,  $n_2 = 1.2887$ ,  $\theta_0 = 80^\circ$ , nm and  $N = 4$ )

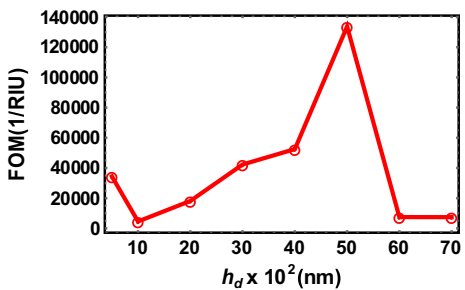
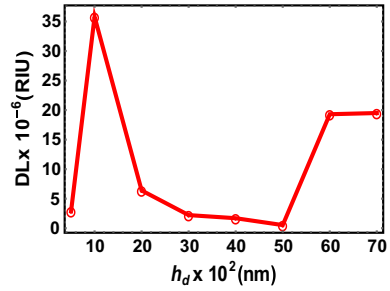


**Fig. 11** Detection Limit (DL) vs the defect cavity thickness ( $h_d$ ) of a proposed binary photonic crystal for TE mode at ( $h_1=106.38$  nm,  $h_2=349.18$  nm,  $n_1=4.23$ ,  $n_2=1.2887$ ,  $\theta_0=80^\circ$ , nm and  $N=4$ )



Furthermore, it is obvious that the value of the detection limit fluctuates as the thickness of the defect cavity increases. The suggested detector has a DL of  $5.2610 \times 10^{-7}$  RIU at a defect cavity thickness of 5000 nm, as shown in Fig. 11.

The low value of DL indicates that the suggested biosensor is capable of detecting even minor changes in the sensing layer’s refractive index. It’s worth noting that raising the defect cavity thickness above  $h_d=5000$  nm results in a small increase in sensitivity. According to all of the parameters of S, QF, FOM, and DL, the best defect cavity thickness is  $h_d=5000$  nm. This thickness is equal  $5 \mu\text{m}$ . By the way, the thickness of biological examination samples is often in micrometers. Therefore, it is preferable that the thickness of the sensing layer be in micro, and this is in agreement with many recently published researches (Daher et al. 2022b; Aly and Zaky 2019).

From the above analysis, we can conclude that performance of the suggested biosensor depending upon the thickness of defect cavity. The increase in the thickness of defect cavity leads to a significant improvement in performance parameters of the optical detector but that is not at all. The best efficiency of the detector is obtained at a certain thickness (optimal thickness), and then the performance declines with the increase in the thickness of cavity. In our proposed detector, the optimal thickness is found at 5000 nm.

When the normal cells of diabetes (NCD) and affected cells of diabetes (ECD) are treated as defect cavities in the suggested structure under the optimal circumstances, the expanded view of the transmittance spectra of the proposed BPhC is shown in Fig. 12. The defect peak is located at 1926.23 nm when the NCD is used as a defect cavity. When affected cells of diabetes (ECD) are used as a defect cavity, the defect peak shifts towards a higher wavelength of 2086.69 nm. The optimum sensitivity is calculated and

**Fig. 12** Transmittance spectra of a BPhC for TE wave at ( $h_1=106.38$  nm,  $h_2=349.18$  nm,  $h_d=5000$  nm,  $n_1=4.23$ ,  $n_2=1.2887$ ,  $\theta_0=80^\circ$ , nm and  $N=4$ )

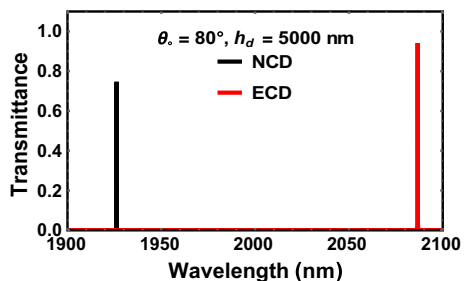


**Table 7** Comparison performance of our detector with performance of the most recent biosensors

Ref	Techniques/structures	S (nm/RIU)	QF	FOM (RIU <sup>-1</sup> )	DL (RIU)
Arafa et al. (2017)	Infiltrated photonic crystal cavity for biosensing	462	$1.1 \times 10^5$	1117	–
Lu et al. (2018)	A dielectric-metal metasurface based an optical sensor	840	1264	84	–
Panda et al. (2021)	Design of biosensor based on a photonic crystal	1016.3	–	–	$2.28 \times 10^{-4}$
Suthar and Bhargava (2021)	Malaria sensor using One-dimensional photonic crystals	495.73	–	–	$8.07 \times 10^{-6}$
Sani et al. (2021)	Optical Microstructure based biosensor for cancer and diabetic cells	2214	946.50	1164.5	–
<b>This work</b>	<b>Design a biosensor based on BPhC for detecting diabetes-affected cells</b>	<b>2676.66</b>	<b>104,337.5</b>	<b>133,833.3</b>	<b><math>5.26 \times 10^{-7}</math></b>

then found as 2676.66 nm/RIU. Here, a high incident angle was employed as well as a high thickness of the defect cavity was considered. Also, the proposed photonic structure contained two periodic layers, the difference between their refractive indices being slightly large. As a result, the suggested detector achieves an ultra-high performance which is not achieved by many existing structures and approaches in this sector. Overall, Table 7 shows that the performance of our suggested biosensor is superior to that of these recently reported publications. Other advantages, the described detector features a simple structure, quick real-time detection, and a customizable design, making it an appropriate tool for diabetes diagnosis. Using the nanoimprint lithography technology, the suggested photonic structure can be produced with easily. The photonic crystal can be incorporated into a waveguide to describe the built system. A micro-gap is introduced between two equivalent numbers of cells can be treated as a defect cavity. The gap is filled with the analyte, and the structure is illuminated by a light source. To exhibit and examine the transmitted beam, an optical detector is necessary on the other side of the structure.

## 4 Conclusion

A biosensor based on a binary photonic crystal (BPhC) has been created for the detection of diabetes. The transmittance domains of the suggested structure are inspected using the transfer matrix approach. The developed biosensor is made of two layers of Ge and TiN that alternate, with the defect cavity acting as the sensing sample. The effect of changing the incidence angle and the cavity thickness on the performance of the suggested structure was examined. By moving the sensing sample from normal to sick cells, the defect peak is transferred to a higher wavelength. TE polarization outperforms TM polarization as the angle of incidence grows. In addition, increasing the defect cavity thickness improved the sensitivity of the suggested biosensor significantly. Our suggested biosensor has a high sensitivity of 2676.66 nm/RIU when the parameters are tuned. Furthermore, the suggested structure had a very high QF (104,337.5), a very high FOM (133,833.3 RIU<sup>-1</sup>), and a very low DL (5.26 × 10<sup>-7</sup>) RIU. Finally, the described detector features a simple structure, quick real-time detection, and a customizable design, making it an appropriate tool for diabetes diagnosis.

**Acknowledgements** The authors would like to acknowledge the support received from Taif University Researchers Supporting Project Number (TURSP-2020/147), Taif university, Taif, Saudi Arabia.

**Data availability** Not Applicable.

## Declarations

**Conflict of interest** All the authors approved for this submission as well as no competing interests.

## References

Almawgani, A.H., Taya, S.A., Daher, M.G., Colak, I., Wu, F., Patel, S.K.: Detection of glucose concentration using a surface plasmon resonance biosensor based on barium titanate layers and molybdenum disulfide sheets. *Phys. Scripta* (2022). <https://doi.org/10.1088/1402-4896/ac68ad>


- Almawgani, A.H.M., Daher, M.G., Taya, S.A., et al.: Highly sensitive nano-biosensor based on a binary photonic crystal for cancer cell detection. *Opt. Quant. Electron* **54**, 554 (2022b). <https://doi.org/10.1007/s11082-022-03978-0>
- Aly, A.H., Zaky, Z.A.: Ultra-sensitive photonic crystal cancer cells sensor with a high-quality factor. *J. Pre-Proofs* **104**(4), 102991 (2019)
- Aly, A.H., Elsayed, H.A., Malek, C.: Defect modes properties in one-dimensional photonic crystals employing a superconducting nanocomposite material. *Opt. Appl.* **48**, 53–64 (2018)
- Amiri, I.S., Yupapin, P., Palai, G.: Estimation of concentration of DNA and protein through PARD and modified analysis: a realization of an accurate biomedical device using photonic structure. *Optik* **182**, 507–511 (2019)
- Arafa, S., Bouchemat, M., Bouchemat, T., Benmerkhi, A., Hocini, A.: Infiltrated photonic crystal cavity as a highly sensitive platform for glucose concentration detection. *Opt. Commun.* **384**, 93–100 (2017)
- Avsar, A., Vera-Marun, I.J., Tan, J.Y., Watanabe, K., Taniguchi, T., Castro Neto, A.H., Ozyilmaz, B.: Air-stable transport in graphene-contacted, fully encapsulated ultrathin black phosphorus-based field-effect transistors. *ACS Nano* **9**(4), 4138–4145 (2015)
- Bommer, C., Heesemann, E., Sagalova, V., Manne-Goehler, J., Atun, R., Bärnighausen, T., Vollmer, S.: The global economic burden of diabetes in adults aged 20–79 years: a cost-of-illness study. *Lancet Diabetes Endocrinol.* **5**(6), 423–430 (2017)
- Chow, E., Grot, A., Mirkarimi, L.W., Sigalas, M., Girolami, G.J.: Ultracompact biochemical sensor built with two-dimensional photonic crystal microcavity. *Opt. Lett.* **29**(10), 1093–1095 (2004)
- Daher, M.G., Taya, S.A., Colak, I., Ramahi, O.M.: Design of a novel optical sensor for the detection of waterborne bacteria based on a photonic crystal with an ultra-high sensitivity. *Opt. Quant. Electron.* **54**(2), 1–18 (2022a)
- Daher, M.G., Taya, S.A., Colak, I., Vigneswaran, D., Olaimat, M.M., Patel, S.K., Ramahi, O.M., Almawgani, A.H.: Design of a nano-sensor for cancer cell detection based on a ternary photonic crystal with high sensitivity and low detection limit. *Chin. J. Phys.* **77**, 1168–1181 (2022b)
- Elsayed, H.A., Sharma, A., Alrowaili, Z.A., Taha, T.A.: Theoretical investigation of pressure sensing using a defect of polystyrene inside photonic crystals. *Mater. Chem. Phys.* **270**, 124853 (2021)
- Frischeisen, J., Mayr, C., Reinke, N.A., Nowy, S., Brütting, W.: Surface plasmon resonance sensor utilizing an integrated organic light emitting diode. *Opt. Express* **16**(22), 18426–18436 (2008)
- Fu, Z., Sun, F., Wang, C., Wang, J., Tian, H.: High-sensitivity broad free-spectral-range two-dimensional three-slot photonic crystal sensor integrated with a 1D photonic crystal bandgap filter. *Appl. Opt.* **58**(22), 5997–6002 (2019)
- Harding, P.J., Euser, T.G., Vos, W.L.: Identification of competing ultrafast all-optical switching mechanisms in Si woodpile photonic crystals. *JOSA B* **26**(4), 610–619 (2009)
- Haxha, S., Jhoja, J.: Optical based noninvasive glucose monitoring sensor prototype. *IEEE Photonics J.* **8**(6), 1–11 (2016)
- Lu, X., Zhang, T., Wan, R., Yongtao, Xu., Zhao, C., Guo, S.: Numerical investigation of narrowband infrared absorber and sensor based on dielectric-metal metasurface. *Opt. Express* **26**(8), 10179–10187 (2018)
- Panda, A., Sarkar, P., Palai, G.: Research on SAD-PRD losses in semiconductor waveguide for application in photonic integrated circuits. *Optik* **154**, 748–754 (2018)
- Panda, A., Pukhrambam, P.D., Keiser, G.: Realization of sucrose sensor using 1D photonic crystal structure vis-à-vis band gap analysis. *Microsyst. Technol.* **27**(3), 833–842 (2021)
- Qin, F., Meng, Z.-M., Li, Z.-Y.: Design of all-optical switching component based on pillar-array hybrid nonlinear photonic crystal cavity. *JOSA B* **29**(9), 2314–2319 (2012)
- Ramanujam, N.R., Amiri, I.S., Taya, S.A., Olyae, S., Udaiyakumar, R., Pasumpon Pandian, A., Joseph Wilson, K.S., Mahalakshmi, P., Yupapin, P.P.: Enhanced sensitivity of cancer cell using one dimensional nano composite material coated photonic crystal. *Microsyst. Technol.* **25**(1), 189–196 (2019)
- Sánchez, A., Orozco, S.: Elasto-optical effect on the band structure of a one-dimensional photonic crystal under hydrostatic pressure. *JOSA B* **33**(7), 1406–1410 (2016)
- Sani, M.H., Sami, P., Shen, C., Behzadnia, H.: High resolution biosensor with simultaneous detection of two refractive index sample in optical microstructure. *J. Res. Sci. Eng. Technol.* **9**(03), 64–75 (2021)
- Suthar, B., Bhargava, A.: Biosensor application of one-dimensional photonic crystal for malaria diagnosis. *Plasmonics* **16**(1), 59–63 (2021)
- Tang, J.-L., Wang, J.-N.: Chemical sensing sensitivity of long-period grating sensor enhanced by colloidal gold nanoparticles. *Sensors* **8**(1), 171–184 (2008)

- Taya, S.A., Daher, M.G., Colak, I., Ramahi, O.M.: Highly sensitive nano-sensor based on a binary photonic crystal for the detection of mycobacterium tuberculosis bacteria. *J. Mater. Sci.: Mater. Electron.* **32**(24), 28406–28416 (2021)
- Taya, S.A., Sharma, A., Doghmosh, N., Colak, I.: Detection of water concentration in ethanol solution using a ternary photonic crystal-based sensor. *Mater. Chem. Phys.* (2022). <https://doi.org/10.1016/j.matchemphys.2022.125772>
- Threm, D., Nazirizadeh, Y., Gerken, M.: Photonic crystal biosensors towards on-chip integration. *J. Biophotonics* **5**(8–9), 601–616 (2012)
- Xie, Q., Chen, Y., Li, X., Yin, Z., Wang, L., Geng, Y., Hong, X.: Characteristics of D-shaped photonic crystal fiber surface plasmon resonance sensors with different side-polished lengths. *Appl. Opt.* **56**(5), 1550–1555 (2017)
- Zhang, J.-P., Li-Ping, Yu.: Preparation of three-dimensional ordered macroporous Cu<sub>2</sub>O film through photonic crystal template-assisted electrodeposition method. *J. Mater. Sci.: Mater. Electron.* **25**(12), 5646–5651 (2014)
- Zyoud, S.H., Ahmed, N.M., Lahewil, A.S., Omar, A.F.: Micro spot ZnO nanotubes using laser assisted chemical bath deposition: a low-cost approach to UV photodetector fabrication. *Sens. Actuators A Phys.* **338**, 113485 (2022)

**Publisher's Note** Springer Nature remains neutral with regard to jurisdictional claims in published maps and institutional affiliations.

Springer Nature or its licensor holds exclusive rights to this article under a publishing agreement with the author(s) or other rightsholder(s); author self-archiving of the accepted manuscript version of this article is solely governed by the terms of such publishing agreement and applicable law.

## Authors and Affiliations

Malek G. Daher<sup>1</sup> · Zbigniew Jaroszewicz<sup>2,3</sup> · Samer H. Zyoud<sup>4,5,6</sup> · Abinash Panda<sup>7</sup> · SK Hasane Ahammad<sup>8</sup> · Mohammed Abd-Elnaby<sup>9</sup> · Mahmoud M. A. Eid<sup>10</sup> · Ahmed Nabih Zaki Rashed<sup>11</sup> 

Malek G. Daher  
malekjbreel20132017@gmail.com

Zbigniew Jaroszewicz  
mmtzjaroszewicz@post.pl

Samer H. Zyoud  
s.zyoud@ajman.ac.ae

Abinash Panda  
abinashpanda087@gmail.com

S K Hasane Ahammad  
ahammadklu@gmail.com

Mohammed Abd-Elnaby  
maahmed@tu.edu.sa

Mahmoud M. A. Eid  
m.elfateh@tu.edu.sa

<sup>1</sup> Physics Department, Islamic University of Gaza, P.O. Box 108, Gaza, Palestine

<sup>2</sup> Department of Physical Optics, Institute of Applied Optics, Warsaw, Poland

<sup>3</sup> National Institute of Telecommunications, Warsaw, Poland

<sup>4</sup> Department of Mathematics and Sciences, Ajman University, Ajman, United Arab Emirates

<sup>5</sup> Nonlinear Dynamics Research Center (NDRC), Ajman University, Ajman, United Arab Emirates

<sup>6</sup> School of Physics, Universiti Sains Malaysia, 11800 Penang, Malaysia

- <sup>7</sup> Department of Electronics and Communication Engineering, National Institute of Technology Silchar, Silchar, Assam 788010, India
- <sup>8</sup> Department of ECE, Koneru Lakshmaiah Education Foundation, Vaddeswaram, Andhra Pradesh 522302, India
- <sup>9</sup> Department of Computer Engineering, College of Computers and Information Technology, Taif University, P.O. Box 11099, Taif 21944, Saudi Arabia
- <sup>10</sup> Department of Electrical Engineering, College of Engineering, Taif University, P.O. Box 11099, Taif 21944, Saudi Arabia
- <sup>11</sup> Electronics and Electrical Communications Engineering Department, Faculty of Electronic Engineering, Menoufia University, Menouf 32951, Egypt